Polymer Testing 30 (2011) 140–149

Contents lists available at ScienceDirect

Polymer Testing

journal homepage: www.elsevier.com/locate/polytest

Test Method

Non-contact technique for characterizing full-field surface deformation of shape memory polymers at elevated and room temperatures

A.J.W. McClung [a,b,*], G.P. Tandon [a,c], K.E. Goecke [a,c], J.W. Baur [a]

[a] Air Force Research Laboratory, Materials and Manufacturing Directorate, Wright-Patterson AFB, OH 45433, USA
[b] National Research Council, USA
[c] University of Dayton Research Ins., 300 College Park, Dayton, OH 45469, USA

ARTICLE INFO

Article history:
Received 7 October 2010
Accepted 17 November 2010

Keywords:
Shape memory polymers
Digital image correlation
Poisson's ratio
Hencky strain
Non-contact methods

ABSTRACT

Thermally activated shape memory polymers (SMPs) can display modulus changes of approximately three orders of magnitude in transitioning from the high modulus, "glassy" state below the glass transition temperature (T_g) to the low modulus, "rubbery" state above the T_g. In the high temperature region, SMPs can achieve strain levels well above 100%. Their complex behavior includes large modulus changes to as low as ~1 MPa, extremely high strain levels, and path dependent properties, thus precluding the use of traditional strain gages and low-contact force extensometers. The present study presents a comparison of thermomechanical testing techniques developed to characterize the material behavior of SMPs. Specifically, the performance of strain measurements using contact methods (clip-on extensometers and adhesive strain gages) are compared to non-contact methods (laser extensometer and digital image correlation). An MTS environmental chamber with an observation window allows for non-contact optical measurements during testing. A series of tensile tests are performed on a commercial SMP (with a T_g of ~105 °C) at 25 °C and at 130 °C. It is observed that the clip-on extensometer significantly affects the SMP behavior even in the low temperature, high modulus state. Overall, the laser extensometer provides a robust method for controlling the axial strain in the gage section of the samples at moderate strain rates. The digital image correlation allows for full field measurement of both axial and transverse strains of SMPs over a range of temperatures and strain rates.

1. Introduction

Thermally activated shape memory polymers (SMPs) show great promise in reconfigurable structures as they exhibit the ability to withstand large deformations and then recover to the original undeformed state [1]. SMPs exhibit a relatively stiff modulus below their glass transition temperature (T_g), and a decrease in modulus by several orders of magnitude when heated above their T_g. In this high temperature state, a high-strain to failure can be achieved. The high flexibility of this state allows the material to be deformed to a new configuration (often to levels up to 400% strain [2]), and "locked in" through cooling the sample back below the T_g. The original state can then be recovered by reheating the material above its T_g without mechanical constraints. Beloshenko et al. [3] provided a review of heat triggered SMPs and listed several advantages of these materials over shape memory alloys, such as low density, high strain-recovery ability, processability and relative low cost. These SMP materials show great promise as the matrix for reconfigurable structures. However, before such applications can be attempted, the 3-D mechanical behavior of SMPs must be thoroughly understood. By understanding critical

* Corresponding author. Air Force Research Laboratory, Materials and Manufacturing Directorate, Wright-Patterson AFB, OH 45433, USA. Tel.: +937 904 4674; fax: +1 937 656 4706.
E-mail address: mcclunga2@asme.org (A.J.W. McClung).

0142-9418/$ – see front matter © 2010 Elsevier Ltd. All rights reserved.
doi:10.1016/j.polymertesting.2010.11.010

mechanical performance at temperatures below, above and through the T_g, the "memory" capabilities of SMPs can enable reconfigurable structures such as micro air vehicles, morphing aircraft and deployable space structures.

The key technical challenge in characterizing the SMP behavior is that traditional contact methods of measuring deformation are not practical for the low modulus and high strain capability of SMPs above their T_g. A "low contact force" high-temperature extensometer can measure engineering strains of +/− 20% and applies a force of 0.9 N to the sample [4]. SMPs can deform over 100% engineering axial strain before failure and will distort under the 0.9 N of contact force when in the high temperature "rubbery" regime. Optical methods have been previously employed to provide measurements of the axial deformation of SMPs [5,6]. However, these experiments have been limited to axial strain, whereas transverse strain measurements have been ignored. In addition, to date, strain control testing has not been achieved on these thermally triggered SMPs above their T_g. Instead, crosshead displacement control, which does not account for localized deformations or the grip thermal expansion/contraction, has been employed. The laser extensometer which has been used in a few of these studies [7–9] as a passive measurement device appears promising for strain control at moderate strain rates with these materials.

Digital image correlation (DIC) refers to a non-contact deformation measurement technique which tracks the distortion of surface patterns on an object during deformation and/or rigid body motion. The images are then post processed to extract full-field deformations. In the current research, a random array pattern on the face of a sample is tracked during axial tension using a stereo view produced from two angularly offset cameras. During processing of the stored images, the DIC system tracks sub-regions of the random array in each image set. By tracking these sub-regions in both cameras, the system calculates a full-field measurement of the local deformations in the x-, y- and z-axis on the face of the sample. These local deformations are then used to determine the 2-D strains on the face of the sample. Great detail is given by Sutton et al. [10] on the methods used in the DIC system to track and calculate the full-field deformation.

DIC has been previously employed to study small deformation in polymeric materials at low temperatures [11,12]. However, significantly less work has been completed on materials exhibiting large strain. Jerabek et al. [12] conducted an extensive study of the effects of the various parameters (e.g., light intensity, shutter time and speckle pattern structure or size) in setting up the DIC system. In their work, they determined that the use of a non-contact optical measurement device is advantageous for determining Poisson's ratio values for polymeric materials exhibiting strain up to 60%. However, they used nominal strain values in their investigations of a polymer with a relatively high modulus (analogous to SMPs at low temperatures). The current investigation applies DIC on highly flexible materials at elevated temperatures where initial data [13] has shown that the shape memory material exhibited nonlinear stress-strain curves similar to elastomeric materials. Previous data did not incorporate a measurement of the transverse strain [13]. Therefore, the Poisson's ratio of the materials as they are deformed in their low modulus state was not determined.

In the present work, the objective is to develop a method to accurately measure the axial and transverse stress-strain behavior of SMPs in both their low temperature "glassy" regime and their high temperature "rubbery" regime. The "rubbery" regime, of course, provides the greater challenge in that the material can deform well above 100% strain in a highly inelastic behavior. Typically, constitutive models for SMPs assume that the Poisson's ratio at a given temperature is a constant and independent of the strain (for example [13]). In the case of deformations of the order of 100%, the constant Poisson's ratio assumption only holds if the Hencky strain definition is employed in the "rubbery" regime [14]. Therefore, the current work examines the influence that temperature and strain level have on the Poisson's ratio using small strain (i.e., Cauchy strain) and large strain (i.e. Green and Hencky strain) definitions. The measured SMP behavior is employed to establish Hencky strain as the appropriate formulation for describing the constitutive response of SMPs throughout the full shape memory cycle (SMC).

2. Measure of strain and Poisson's ratio

Strain is a measure of the relative displacement of material elements (without rigid body motion) within a structure. There are many measures of strain. The proper description of strain is both fundamental and necessary to avoid misrepresentation of the mechanical response of the material. In the current study, the three strains discussed are the Cauchy, Green and Hencky strains, which are briefly reviewed. Consider uniaxial tension of a uniform bar with homogeneous and isotropic properties and initial length l_0. If we stretch the bar to a new length l, we can define the stretch ratio as

$$\lambda_1 = \frac{l}{l_0}. \tag{1}$$

Axial strain is then defined as a function of λ_1. The most common axial strain definition is the Cauchy strain

$$\varepsilon_1^C = \frac{l - l_0}{l_0} = \lambda_1 - 1. \tag{2}$$

The Cauchy strain (also known as engineering strain) is used when dealing with small deformations where the undeformed and deformed configurations of the body can be assumed nearly identical. (In this case, the nonlinear terms of the finite strain tensor can be ignored.)

When dealing with finite elastic deformations, the undeformed and deformed configurations are distinctly different. Therefore, the nonlinear terms must be included. The Green strain ε_1^Gincludes the nonlinear elastic terms of the finite strain tensor.

$$\varepsilon_1^G = \frac{l^2 - l_0^2}{2l_0^2} = \frac{1}{2}\left(\lambda_1^2 - 1\right) \tag{3}$$

For the case of large inelastic deformations involving path dependent and non-recoverable strains, the Hencky strain ε_1^H is an appropriate strain measure.

$$\varepsilon_1^H = \int_{l_0}^{l} \frac{dl}{l} = In\frac{l}{l_0} = In(\lambda_1) \tag{4}$$

Note that the Hencky strain integrates the incremental strain (dl/l), providing a path dependent measure of the deformation.

All three of these measures meet the requirement of a strain function to reduce to zero at $\lambda_1 = 1$. A graphical comparison of the strain measures is shown in Fig. 1. For values of λ_1 near 1, the three strain measures are similar. However, for larger deformations the strain measures differ greatly.

Poisson's ratio ν provides a measure of the negative of the transverse contraction over the axial stretch under a given axial tensile stress σ_1. The standard ν is defined as

$$\nu = -\frac{\varepsilon_2(\sigma_1)}{\varepsilon_1(\sigma_1)}. \tag{5}$$

In this definition, ν depends on the strain measure used (i.e., $\varepsilon_2^C/\varepsilon_1^C \neq \varepsilon_2^G/\varepsilon_1^G \neq \varepsilon_2^H/\varepsilon_1^H$ with increasing sophistication of non-linearity).

For the case of an isotropic material,

$$\lambda_2 = \lambda_3 \tag{6}$$

and for incompressibility

$$\lambda_1\lambda_2\lambda_3 = 1. \tag{7}$$

Combining Eqs. 6 and 7 it follows that

$$\lambda_2 = \lambda_1^{-1/2}, \tag{8}$$

which can be combined with Eq. (5) to obtain the following expressions for the Cauchy, Green and Hencky Poisson's ratios respectively for an incompressible isotropic material:

$$\nu^C = -\frac{\varepsilon_2^C(\sigma_1)}{\varepsilon_1^C(\sigma_1)} = \frac{1-\lambda_2}{\lambda_1-1} = \frac{1-\lambda_1^{-\frac{1}{2}}}{\lambda_1-1} = \frac{1}{\lambda_1+\lambda_1^{(1/2)}} \tag{9}$$

$$\nu^G = -\frac{\varepsilon_2^G(\sigma_1)}{\varepsilon_1^G(\sigma_1)} = -\frac{\frac{1}{2}\left(\lambda_2^2-1\right)}{\frac{1}{2}\left(\lambda_1^2-1\right)} = \frac{1}{\lambda_1^2+\lambda_1} \tag{10}$$

$$\nu^H = -\frac{\varepsilon_2^H(\sigma_1)}{\varepsilon_1^H(\sigma_1)} = -\frac{In(\lambda_2)}{In(\lambda_1)} = -\frac{In\left(\lambda_1^{-\frac{1}{2}}\right)}{In(\lambda_1)} = \frac{1}{2} \tag{11}$$

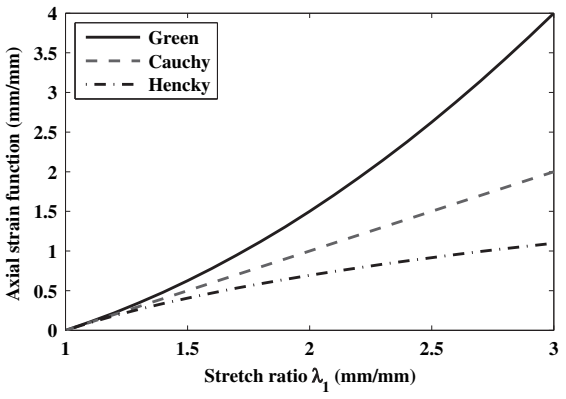

Fig. 1. Strain measures as a function of λ_1.

A graphical comparison of ν for an incompressible material for the various strain measures is presented in Fig. 2. Note that $\nu = 0.5$ and is independent of λ_1 only if Eq. (11) is used.

These definitions of strain and ν provide valuable insight which will be revisited below in relation to the SMP behavior measured in the low and high temperature regimes. Experimental results will be evaluated in terms of which strain formulation is valid for describing the constitutive behavior of SMP materials. The results will demonstrate that the Hencky strain formulation is the optimal choice for describing SMPs in their "rubbery" state. In the "glassy" state, the stretch ratio is small enough that the three formulations collapse toward each other (see λ_1 below 1.5 in Fig. 1), however, as we will demonstrate later, the Veriflex-E at room temperature exhibits strains at failure approaching 14% axial Cauchy strain. This same strain level corresponds to 13.10% Hencky and 14.98% Green strain. Therefore, even for the room temperature SMP, the difference between the strain values differ enough to warrant thoughtful selection of the strain formulation. For consistency with the requirements of SMPs in their "rubbery" regime, the results in the current paper are presented in Hencky strain and true stress unless otherwise indicated.

3. Experimental setup

Validation of the experimental measurements was conducted using common metal and rubber materials, while highlighting the limitations and errors introduced by employing the more common Green and Cauchy strain formulations.

3.1. Material

To verify the ability of the DIC system to accurately measure small strains such as those observed in SMPs in their low temperature "glassy" regime, strain measurements were conducted using 6061 grade aluminum coupons of thickness 1.65 mm. The aluminum was machined into a dumbbell shaped specimen (total length = 115 mm,

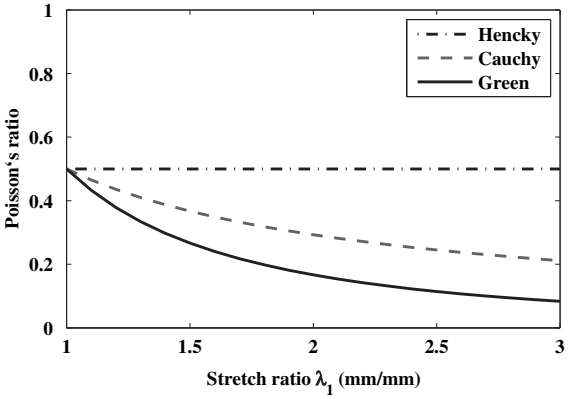

Fig. 2. Poisson's ratio measures for the various strain formulations for an incompressible material as a function of λ_1.

overall width = 19 mm, gage length = 25 mm, width of narrow section = 6 mm) in accordance with ASTM-D 638.

Similarly, the ability to accurately measure large strains was verified using Styrene-Butadiene-Rubber (SBR) for which both the axial and transverse strain data is available in the published literature [14]. Dumbbell shaped samples were cut from rubber sheets with a punch (total length = 63.5 mm, overall width = 19 mm, gage length = 12.7 mm, width of narrow section = 3.1 mm, thickness = 2 mm). A smaller sample size was selected in order to accommodate the potential axial deformation above 600% nominal (Cauchy) strain for elastomers inside of the environmental chamber.

The SMP studied was Veriflex-E, a two-part epoxy based resin manufactured by Cornerstone Research Group, Inc. (CRG). The material was purchased from CRG with a designed T_g of 105 °C. Panels of neat resin were fabricated in sealed molds between glass plates. The samples were cured in a convection oven following the manufacturer recommended cure cycle. Dumbbell shaped test specimens (again following ASTM-D 638, total length = 115 mm, overall width = 19 mm, gage length = 25 mm, width of narrow section = 6 mm) were machined from the 3-mm thick panel using waterjet machining. The material was post-cured for 30 min at 150 °C as recommended in Tandon et al. [15] and McClung et al. [16] before testing.

3.2. MTS load frame and environmental chamber

Tensile tests were conducted on an MTS machine surrounded by an MTS 651 environmental chamber with a glass window for making optical measurements inside the chamber. A 15 kN water-cooled load cell and MTS Advantage 2 kN pneumatic grips were used for the aluminum and the SMP low temperature (25 °C) experiments to a resolution of 15 N. An 890 N water-cooled load cell and MTS Advantage 200 N pneumatic grips were used for the SBR and the SMP high temperature (130 °C) experiments to a resolution of 0.89 N. An MTS FlexTest 40 digital controller was employed for input signal generation and data acquisition. Strain was measured/controlled using the DIC system and laser extensometer as discussed below. In select tests, these strains were compared to those measured by a strain gage or to an MTS 634.11 axial extensometer to demonstrate the accuracy of the laser and DIC measured strains.

For elevated temperature testing, type K thermocouples were attached to test specimens using Kapton tape to verify the furnace calibration on a periodic basis. The environmental chamber controller (using a non-contacting thermocouple exposed to the ambient environment near the test specimen) was adjusted to determine the power setting needed to achieve the desired temperature of the test specimen. The determined power setting was then used in the actual tests. Thermocouples were not attached to the test specimens after the chamber was calibrated so as not to induce any mechanical deformation. A standard temperature ramp rate of 2.5 °C was used for heating/cooling the chamber to the desired temperature with a 60 min total soak time to ensure thermal equilibrium. A typical thermal profile of the chamber and SMP sample with two thermocouples attached is given in Fig. 3a. For thermal calibration, one thermocouple was placed in the middle of the gage section (marked by O in Fig. 3b), and the other thermocouple was placed just outside the laser tape (marked by X in Fig. 3b). The thermocouple temperatures follow closely to the chamber temperature during the initial heat up. There is a small lag between the sample thermocouples and the chamber as it reaches 130 °C. However, an initial 30 min soak time does allow the thermocouples to rise completely to the temperature of the chamber. The extra 30 min of soak time is used to allow the entire SMP gage section to reach the same temperature as the exterior of the sample.

3.3. Laser extensometer

Strain control was accomplished using an MTS laser extensometer with a 25.4-mm gage length to the retro-reflective laser tape applied to each sample. (To the best of our knowledge, this is the first time the signal from the laser extensometer has been used as the active feedback to the controller.) Initial tuning of the controller was conducted with reflective tape on the grips (no sample loaded in the MTS load frame). Fine tuning of the controller was then conducted with the reflective tape applied to a dumbbell shaped sample in the high temperature "rubbery" state. All isothermal tests (unless otherwise indicated) were performed under laser extensometer control with strain rates ranging from 10^{-4} to 10^{-2} s^{-1}. The laser tape is shown with a 25.4-mm gage section on the sample in Fig. 3b.

3.4. Digital image correlation

The full strain field was measured on the face of the sample throughout each test using a Correlated Solutions (CS) DIC system. This system included two "grasshopper" (2 Megapixel) digital cameras focused on the same region of interest but offset by 8° from the perpendicular axis of the sample plane and the CS software to both capture and analyze the images for determining the strain fields. Unless

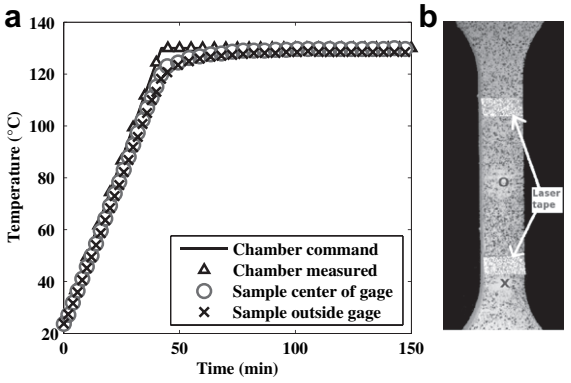

Fig. 3. Measurement of temperature profile during heat up of environmental chamber with a thermocouple on the front side of sample in middle of gage section (O) and a thermocouple on the front side of sample just outside of gage section (×): (a) temperature profile during heat up of environmental chamber and SMP sample (b) location of thermocouples on SMP sample.

otherwise indicated, strain values reported in this article are the strains measured by this DIC system. Two Promaster optical filters type 80A were used on each camera (for a total of four filters) to remove distortion of the DIC data by the laser line created by the extensometer. The effect of the filters is illustrated in Fig. 4. Lighting was provided for the DIC system using a combination of blue LEDs and two 250 W fiber optic lamps external to the environmental chamber.

The optical window of the environmental chamber is comprised of 3 parallel panes of borosilicate glass (Borofloat 33). In order to eliminate the optical refraction caused by the glass, an extra calibration step was included in the testing procedure. This calibration was incorporated using the built in function ("calibrate camera orientation") in the CS software.

A random speckle pattern of high contrast is required for the DIC system to track the full strain field on the face of the sample. For temperatures at or near room temperature, a matte white background layer was spray painted onto the samples. The speckles were then sprayed on using a matte black paint, which gives the resulting effect seen in Fig. 4c. At higher temperatures and moderate strains, the paint was found to degrade and flake off of the sample face. Therefore, high contrast speckles were applied with either a black or a silver permanent marker (depending on the sample color) directly to the face of the samples tested at high temperature, an example permanent marker pattern is shown in Fig. 5.

A detailed discussion about accurate use of the DIC system (as well as a history of photogrammetry and DIC) can be found in [10,17]. The DIC system captures sets of two pictures (one with each camera) which are then post processed using the DIC image software. During post processing,

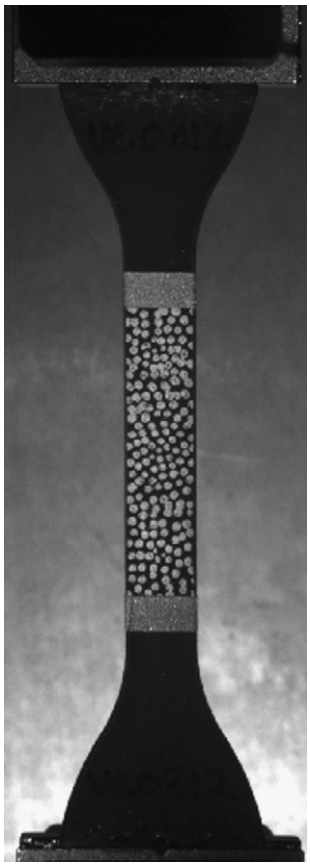

Fig. 5. DIC image with permanent marker speckle pattern.

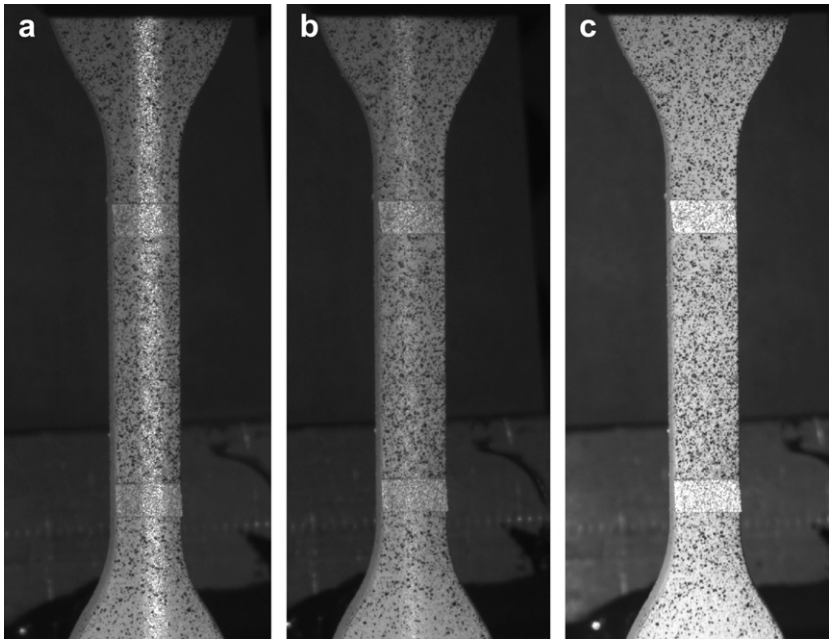

Fig. 4. Effect of 80A filters on the DIC image: (a) No filters, laser illumination is dominant on center axis of sample in the image. (b) One filter on each camera, a small amount of laser illumination is present on center axis of sample in the image. (c) Two filters on each camera, the laser illumination is eliminated in the image.

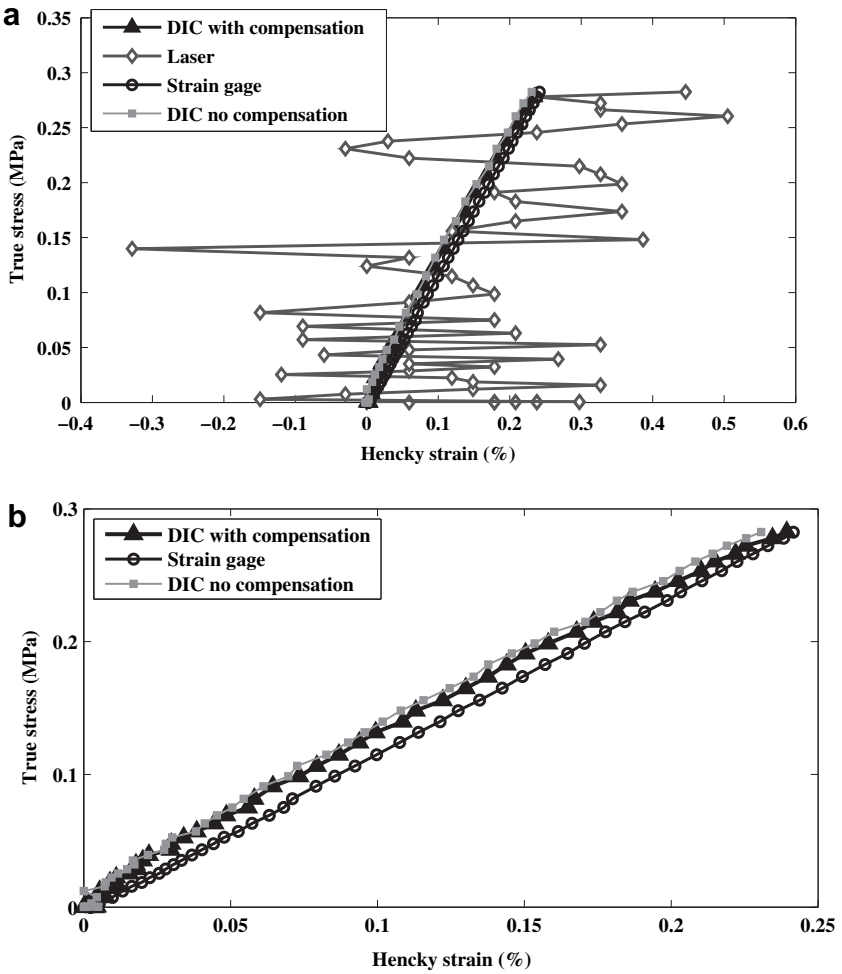

Fig. 6. Stress vs axial strain curves obtained for aluminum 6061 in tensile tests at 25 °C. The DIC calculated strains match well with the strain gage applied to the back of the sample. (a) Laser results included. (b) Zoomed in without laser results.

the system calculates the 2-D strain field on the face of the sample by measuring the displacements from the reference state. The DIC results presented in this paper represent the average strains measured by the DIC within the gage section for each test. Note that the stretch field is assumed to be isotropic in the gage section of the sample $\lambda_2 = \lambda_3$.

4. Experimental results

4.1. Aluminum

The 6061 aluminum was machined into a dumbbell shape and a Vishay Micro-Measurements t-rosette strain gage (CEA-06-032UW-120) was bonded to the gage section of the specimen, providing both axial and transverse strain measurements. The face of the sample without the strain gage was then painted to simultaneously enable DIC measurements. The aluminum sample was strained to the 2 kN force limit of the pneumatic grips at a displacement control rate of 5 mm/min. Although the test was conducted at room temperature, the oven door was kept closed in order to examine the refraction introduced by the glass window. The axial strain gage, laser extensometer and DIC data are shown in Fig. 6a. The laser extensometer shows significant scatter compared to the strain gage and the DIC, indicating that the laser is not as appropriate a measurement method for tests in which particularly small strains are expected in the material. The axial strain gage and DIC data from Fig. 6a are magnified to show greater detail in Fig. 6b. The axial DIC data is shown both with and without the calibration step to compensate for optical refraction through the glass. As seen in Fig. 6b, the axial DIC strain with glass compensation included is in better agreement with the strain gage measurements. In contrast, the DIC measured axial strain without compensation shows a slightly lower strain magnitude than both the compensated DIC and the strain gage data throughout the stress-strain curve. In the current data, the maximum epipolar projection error in the DIC strain measurements without compensation for the glass is 0.045, while the maximum epipolar projection error with compensation for the glass is 0.033. The difference is not dramatic, however, the rule-of-

thumb acceptable epipolar projection error according to CS is within 0.035. The compensation did bring the data from just outside the acceptable error range to inside the acceptable error envelope. In addition, the glass used in this work is high-quality optical glass; if using lesser quality glass, the influence would be greater. In any case where the DIC is used through panes of glass, the optical refraction through the glass should be taken into consideration and the extra compensation step should be considered to ensure accurate strain measurements.

The transverse strain gage and DIC data are shown in Fig. 7. The DIC data is once again shown both with and without the compensation for the optical refraction through the glass. As seen in Fig. 7, the transverse DIC strain with glass compensation included is in reasonable agreement with the strain gage measurements. In contrast, the DIC measured transverse strain without compensation underestimates the strain value throughout the stress-strain curve. These differences illustrate the importance of the compensation which is required to correct for the refraction that occurs through the glass window. Hereafter, any strain data obtained using the DIC method will be shown after it has been corrected for the refraction through the glass window.

The Poisson's ratio calculated using the Hencky strain (Eq. (11)) formulation for the strain gage data and the DIC data is shown in Fig. 8. At the origin (strain ≈ zero), the Poisson's ratio measured by both methods is a small number divided by zero, giving undefined numerical results (NaN). The data does begin to show valid information at approximately 0.05% strain. Both measurement methods approach an average constant Poisson's ratio of approximately 0.3 which is the expected value for aluminum.

4.2. Styrene-Butadiene-Rubber

The mechanical behavior of Styrene-Butadiene-Rubber (SBR) under tensile loading has been examined by Starkova and Aniskevich [14]. These results provide an essential benchmark for the current research to verify accurate use of the DIC technique on an elastomer. In the present study, SBR uniaxial tensile tests were performed at a constant crosshead speed of 25 mm/min. Using the DIC technique, both the axial and transverse strains were measured and the Poisson's ratio computed as a function of stretch ratio using Cauchy, Green and Hencky strain formulations (Eq. (9)–(11) respectively). Fig. 9 compares the results of the present study with the data reported by Starkova and Aniskevich [14] for SBR. There is good agreement between the two data sets over the range of stretch ratio considered. As stated previously, the Poisson's ratio of an incompressible material is a constant only if the Hencky strain definition is used. Use of Cauchy or Green strain produces nonphysical results in which the well known incompressibility of rubber is not supported. These results demonstrate that the non-contact DIC set-up discussed in this work can be effectively used to measure the full strain field on the face of SMPs when they are in their "rubbery" state.

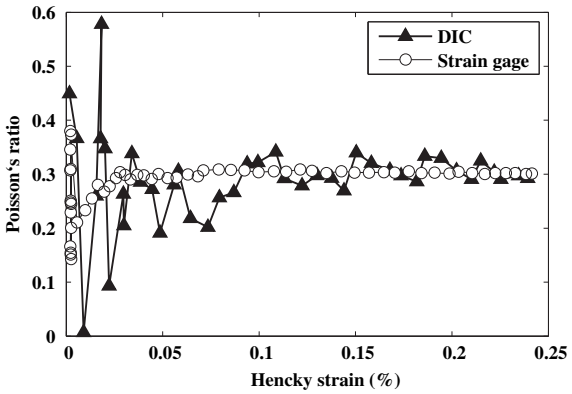

Fig. 8. Poisson's ratio (calculated using Hencky strain) vs axial strain curves obtained for aluminum 6061 in tensile tests at 25 °C. The DIC calculated ratios match well with the strain gage applied to the back of the sample.

4.3. Veriflex-E low temperature regime (25 °C)

Veriflex-E specimens were subjected to strain-controlled tensile tests to failure at 25 °C at a constant strain rate of 10^{-4} s^{-1}. The results are shown in Fig. 10a comparing the

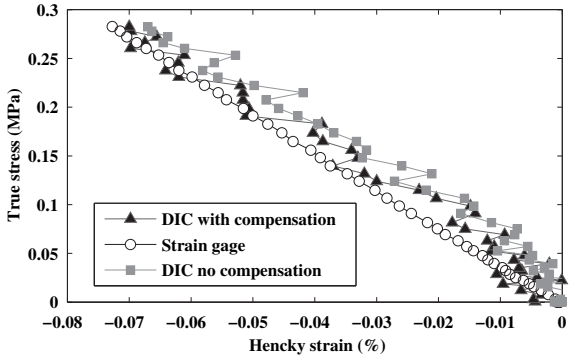

Fig. 7. Stress vs transverse strain curves obtained for aluminum 6061 in tensile tests at 25 °C. The DIC calculated strains match well with the strain gage applied to the back of the sample.

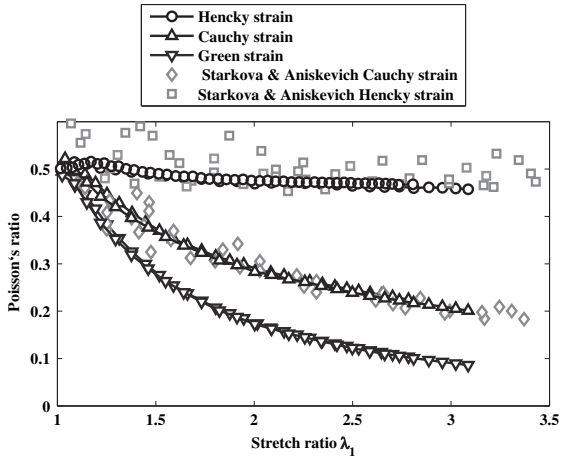

Fig. 9. Styrene-Butadiene-Rubber Poisson's ratio as a function of stretch ratio in the cases of Hencky, Cauchy and Green strains at 25 °C. Results are compared to reproduction of Starkova and Aniskevich [14].

axial strain measurements made via the laser extensometer, the DIC and a "clip-on" extensometer simultaneously on the same specimen. The three measurement methods exhibit excellent agreement up to 8% strain. The differences that are seen at high strains are most likely due to the slight variation in the gage section for the three measurement types. Note in Fig. 10b (a photograph of the specimen during testing with DIC results superimposed) the laser gage length is slightly longer than the clip-on extensometer gage length, and the clip-on extensometer gage length is slightly larger than the DIC gage length. The slight differences in the gage section of the measurements has minimal influence until yielding occurs. At yielding, the dumbbell specimen begins to exhibit higher localized strain near the bottom clip of the extensometer. Thus, the different measurement methods pick up different proportions of this yielding region and, therefore, show slight variations in the calculated strain after yield. These differences in the gage section lengths are necessary to achieve simultaneous measurements with the three methods.

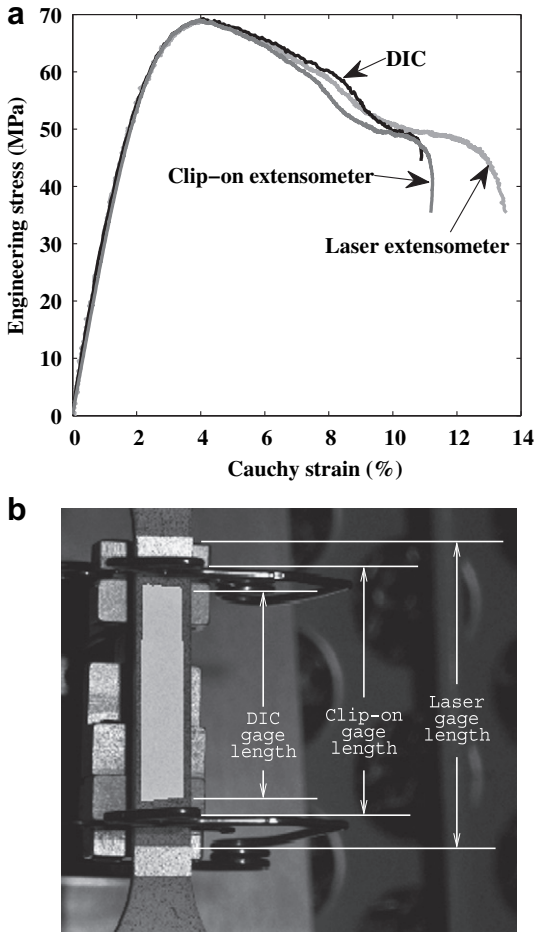

Fig. 10. Veriflex-E in a tensile test to failure conducted at a constant strain rate of 10^{-4} s^{-1} at 25 °C. The DIC calculated strains match well with the clip-on extensometer applied to the back of the sample. (a) Stress-strain curves (b) Photograph of specimen during testing. The laser, clip-on extensometer and DIC gage lengths are marked for comparison.

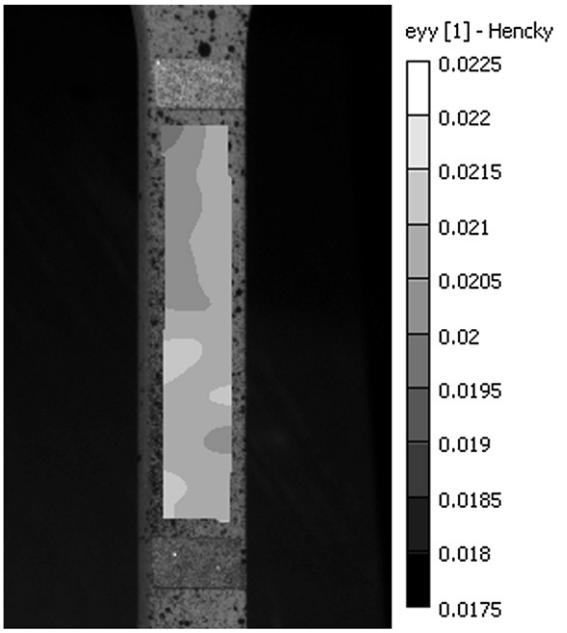

Fig. 11. DIC results at 2% Hencky strain obtained for Veriflex-E during a tensile test conducted at constant strain rate of 10^{-4} s^{-1} at 25 °C.

The uniformity of the strain field measured by the DIC method at 25 °C is illustrated using axial Hencky strain in Fig. 11 at a mean strain level of 2.07% strain. This strain level was chosen such that necking was not yet present in the sample. (The axial strain is signified by eyy[1] in the figure.) The maximum strain measured at this stress level is 2.11% and the minimum is 1.95% strain, producing a spread of 0.11% strain from the mean measured value. The coefficient of variation is 0.0132.

The influence of the clip-on extensometer on the material behavior was explored at strain rates of 10^{-4}, 10^{-3} and

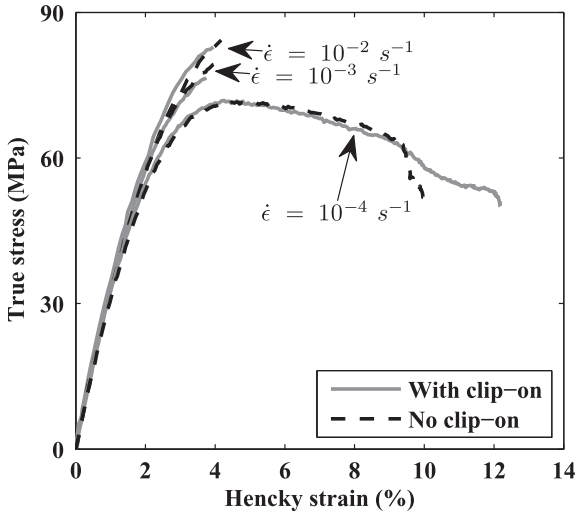

Fig. 12. Stress-strain curves obtained for Veriflex-E in tensile tests to failure conducted at constant strain rates of 10^{-4}, 10^{-3} and 10^{-2} s^{-1} at 25 °C. Results with and without a clip-on extensometer are shown for comparison.

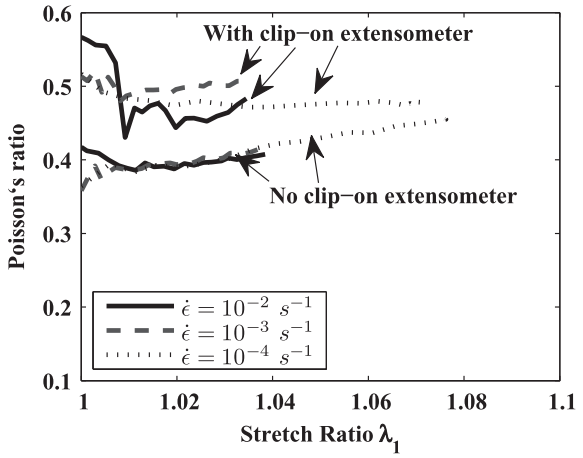

Fig. 13. Poisson's ratio obtained for Veriflex-E in tensile tests to failure conducted at constant strain rates of 10^{-4}, 10^{-3} and 10^{-2} s^{-1} at 25 °C. Results with and without a clip-on extensometer are shown for comparison.

10^{-2} $s^{-1}$with the results shown in Fig. 12. The stress-strain curves obtained at 10^{-3} and 10^{-2} $s^{-1}$are not influenced by the presence of the extensometer. However, at the slowest rate (10^{-4} s^{-1}) the results show a larger strain to failure when the clip-on extensometer is attached to the sample. It was observed that the sample with the clip-on extensometer had two cracks that initiated slowly from opposite edges of the sample and merged during this failure, whereas the other sample without the clip-on extensometer had only a single edge crack. Most likely, the difference in the failure strain is caused by the differing damage as opposed to the presence of the clip-on extensometer.

The DIC technique was also used to measure the transverse strain and the ν^H was computed using Eq. (11). Fig. 13 shows the influence of the clip-on extensometer on the measured ν^H. With the extensometer, the material appears to exhibit $\nu^H = 0.5$. On the contrary, without the presence of the extensometer, Veriflex-E exhibits behavior more akin to expected polymer behavior of $\nu^H = 0.4$ near the origin. As the Veriflex-E is subjected to higher strains, ν^H increases, approaching $\nu^H = 0.5$. Thus, while the measurement of axial strain (see Fig. 12) does not show significant differences of the sample behavior with and without the presence of the clip-on extensometer, the transverse strain and the computed Poisson's ratio are greatly influenced by the presence of the clip-on extensometer, as seen in Fig. 13.

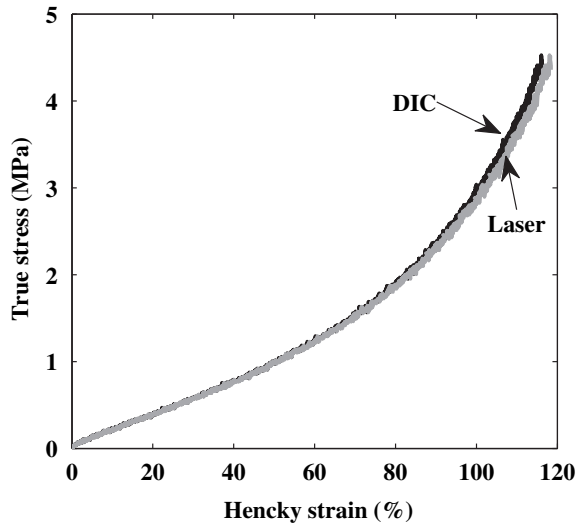

Fig. 14. Stress-strain curves obtained for Veriflex-E in tensile tests to failure conducted at constant strain rate of 10^{-2} s^{-1} at 130 °C. The laser extensometer and DIC are in agreement.

4.4. Veriflex-E high temperature regime (130 °C)

Veriflex-E specimens were subjected to strain-controlled tensile tests to failure tests at 130 °C at constant strain rate of 10^{-2} s^{-1}. For high temperature testing, neither strain gages nor clip-on extensometers are practical for measuring strain because of the low modulus and high strain capability of the SMP in the "rubbery" state. Fig. 14 shows that the DIC and laser extensometer axial strain measurements exhibit excellent agreement throughout the test.

The uniformity of the strain field measured by the DIC at 130 °C is illustrated using axial Hencky strain in Fig. 15 at a mean strain level of 50.9% strain. (The axial strain is signified by eyy[1] in the figure.) The maximum strain measured in this figure is 51.8% and the minimum is 48.7% strain, producing a spread of 2.2% strain from the mean measured value. The coefficient of variation is 0.0127.

The DIC technique was also used to analyze the strain in the transverse direction and the Poisson's ratio determined using Hencky, Cauchy and Green strain formulations. Fig. 16 shows that Veriflex-E exhibits $\nu^H = 0.5$ at the elevated temperature. Note that the Cauchy and Green strain definitions result in a Poisson's ratio which is dependent on the stretch ratio.

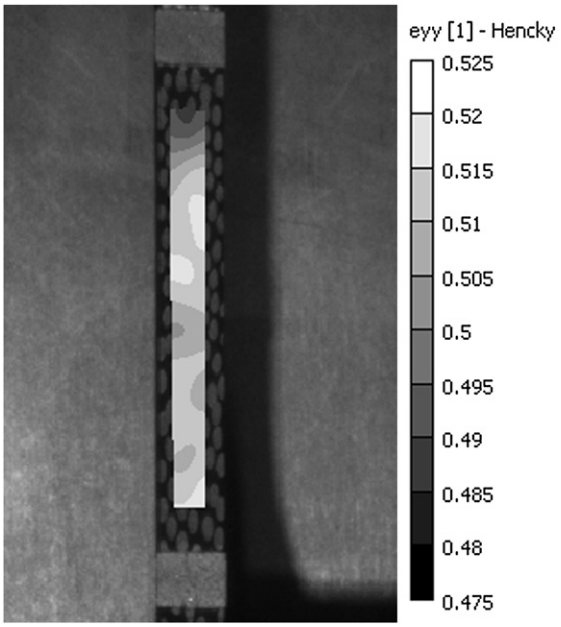

Fig. 15. DIC results at 50% Hencky strain obtained for Veriflex-E during a tensile test conducted at constant strain rate of 10^{-2} s^{-1} at 130 °C.

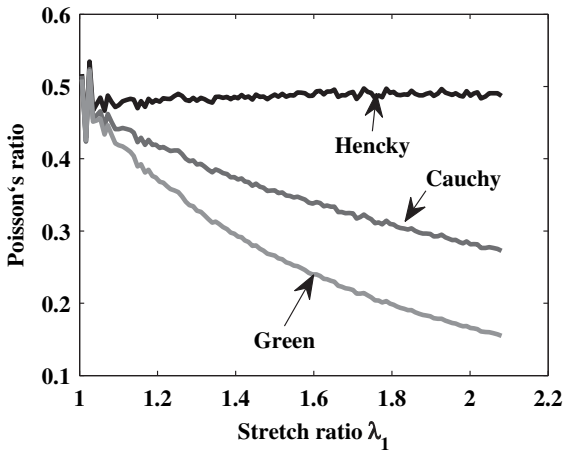

Fig. 16. Poisson's ratio obtained for Veriflex-E in tensile test to failure conducted at constant strain rate of 10^{-2} s^{-1} at 130 °C. Results employing Hencky, Cauchy and Green strains are shown for comparison.

5. Concluding remarks

In this study, the non-contact DIC technique was used to measure the axial and transverse strain of a structural SMP at both room and elevated temperatures. The testing was conducted on an MTS load frame within an environmental chamber. The preliminary experiments have established the validity of the measurements obtained with the DIC system and the laser extensometer while exposing some of the limitations of traditional strain measurement systems.

Significant conclusions on thermomechanical evaluation of SMPs include:

- DIC is preferred for establishing the transverse deformation of SMPs during axial tension. This holds for both high temperature and room temperature testing as the room temperature transverse behavior is strongly influenced by the presence of a clip-on extensometer.
- DIC random speckle pattern should be carefully selected depending on the temperature at which one is testing the SMP so as to remain robust and have sufficient speckle spacing to accurately track the full strain field.
- A correction step is required while using the DIC method on images taken through glass in order to correct for refractions caused by the glass.
- A laser extensometer is ideal for strain controlled testing of SMPs at high temperatures and high strains.
- The use of optical filters enables accurate simultaneous use of the DIC and the laser extensometer for testing SMPs.
- The Hencky definition of strain is required for large deformation formulations in order to assume a Poisson's ratio that is independent of the stretch ratio for incompressible material.
- DIC is an elegant method of mapping the 3-D displacement field of an SMP in a non-contact manner at both low and high temperatures.

Acknowledgment

This research was performed while the primary author held a National Research Council Research Associateship Award at the Air Force Research Laboratory.

References

[1] A. Lendlein, S. Kelch, Shape-memory polymers, Angew. Chem. Int. Ed. 41 (2002) 2035–2057.
[2] J. Leng, H. Lu, Y. Liu, W.M. Huang, S. Du, Shape-memory polymers – a class of novel smart materials, MRS Bull. 34 (2009) 848–855.
[3] V.A. Beloshenko, V.N. Varyukhin, Y.V. Voznyak, The shape memory effect in polymers, Russ. Chem. Rev. 74 (2005) 265–283.
[4] 632.59 High Temperature Axial Extensometers. Data Sheet. MTS Systems Corporation. Available: http://www.mts.com/stellent/groups/public/documents/library/dev_003707.pdf. [accessed 05.10.2010]
[5] B. Atli, F. Gandhi, G. Karst, Thermomechanical characterization of shape memory polymers, J. Intell. Mater. Syst. Struct. 20 (2009) 87–95.
[6] B.L. Volk, D.C. Lagoudas, Y.-C. Chen, Thermomechanical characterization of the nonlinear, rate dependent response of shape memory polymers, Proc. SPIE 6929 (2008).
[7] E.R. Abrahamson, M.S. Lake, N.A. Munshi, K. Gall, Shape memory mechanics of an elastic memory composite resin, J. Intell. Mater. Syst. Struct. 14 (2003) 623–632.
[8] G. McKnight, R. Doty, G. Herrera, C. Henry, Bill Armstrong memorial session: elastic modulus and strain recovery testing of variable stiffness composites for structural reconfiguration applications, Proc. SPIE 6526 (2007).
[9] R. Beblo, K. Gross, L.M. Weiland, Mechanical and curing properties of a styrene-based shape memory polymer, J. Intell. Mater. Syst. Struct. 21 (7) (2010) 677–683.
[10] M.A. Sutton, J.-J. Orteu, H.W. Schreier, Image Correlation for Shape, Motion and Deformation Measurements. Springer, 2009.
[11] G.X. Shen, S.S. Cha, F.-P. Chiang, C.R. Mercer, Digital Image Correlation for Mechanical Behavior of Viscoelastic Materials, vol. 5058, SPIE, 2003.
[12] M. Jerabek, Z. Major, R. Lang, Strain determination of polymeric materials using digital image correlation, Polym. Test. 29 (2010) 407–416.
[13] H.J. Qi, T.D. Ngyuen, F. Castro, C.M. Yakacki, R. Shandas, Finite deformation thermo-mechanical behavior of thermally induced shape memory polymers, J. Mech. Phys. Solids 56 (2008) 1730–1751.
[14] O. Starkova, A. Aniskevich, Poisson's ratio and the incompressibility relation for various strain measures with the example of a Silica-Filled SBR Rubber in uniaxial tension tests, Polym. Test. (2010).
[15] G. Tandon, K. Goecke, K. Cable, J. Baur, Durability assessment of styrene- and epoxy-based shape-memory polymer resins, J. Intell. Mater. Syst. Struct. 20 (2009) 2127–2143.
[16] A. McClung, G. Tandon, D. Foster, J. Baur, Influence of Repeated Cycling and Post-cure on the DMA Characterization of Shape Memory Polymers. In Proc. SAMPE, May 17–20 (2010).
[17] Correlated Solutions, Vic-3D Reference Manual, 2007. www.correlatedsolutions.com.